DOI: 10.6060/ivkkt.20256806.7181

УДК: 537.525

ВЛИЯНИЕ СООТНОШЕНИЯ Ar/He НА СОСТАВ ПЛАЗМЫ И КИНЕТИКУ ТРАВЛЕНИЯ КРЕМНИЯ В CF_4- И C_4F_8- СОДЕРЖАЩИХ ТРЕХКОМПОНЕНТНЫХ СМЕСЯХ

А.М. Ефремов, В.Б. Бетелин, K.-H. Kwon

Александр Михайлович Ефремов (ORCID 0000-0002-9125-0763)*

НИИМЭ, ул. Академика Валиева, 6/1, Зеленоград, Москва, Российская Федерация, 124460
E-mail: amefremov@mail.ru*

Владимир Борисович Бетелин (ORCID 0000-0001-6646-2660)

ФГУ ФНЦ НИИСИ РАН, Нахимовский пр., 36, к. 1, Москва, Российская Федерация, 117218
E-mail: betelin@niisi.msk.ru

Kwang-Ho Kwon (ORCID 0000-0003-2580-8842)

Korea University, 208 Seochang-Dong, Chochiwon, Korea, 339-800
E-mail: kwonkh@korea.ac.kr

Проведено исследование электрофизических параметров плазмы, состава газовой фазы и кинетики реактивно-ионного травления кремния в смесях CF_4 + Ar/He и C_4F_8 + Ar/He с переменным содержанием инертных компонентов. При совместном использовании диагностики плазмы (зонды Лангмюра, оптическая эмиссионная спектроскопия) и моделирования кинетики плазмохимических процессов а) выявлены механизмы влияния соотношения Ar/He на концентрации активных частиц (атомов фтора, полимеробразующих радикалов и положительных ионов), формирующих брутто-результат взаимодействия плазмы с обрабатываемой поверхностью; б) разделены вклады физической и химической составляющих скорости травления; и в) проведен анализ механизма травления в приближении эффективной вероятности взаимодействия. Показано, что общими тенденциями при замещении аргона на гелий в обеих смесях являются снижение температуры и концентрации электронов, уменьшение степеней диссоциации многоатомных частиц, приводящее к аналогичному изменению концентраций менее насыщенных фторуглеродных радикалов и атомов фтора, а также снижение скорости травления кремния, обусловленное изменением кинетики гетерогенной реакции $Si + xF \rightarrow SiF_x$. Изменение эффективной вероятности этой реакции с ростом доли гелия в смеси согласуется со снижением полимеризационной способности в смеси CF_4 + Ar/He, но противоречит росту полимеризационной способности в плазме C_4F_8 + Ar/He. Сделано предположение, что причиной последнего эффекта служит увеличение (по сравнению с величиной, определяемой концентрацией атомов фтора в плазме) потока атомов фтора на границе полимер/кремний. Причиной этого служит генерация атомов фтора в слое полимера увеличивающейся толщины за счет дефторирования под действием ионной бомбардировки.

Ключевые слова: фторуглеродные газы, аргон, гелий, плазма, параметры, активные частицы, ионизация, диссоциация, травление, вероятность реакции

Для цитирования:

Ефремов А.М., Бетелин В.Б., Kwon K.-H. Влияние соотношения Ar/He на состав плазмы и кинетику травления кремния в CF_4- и C_4F_8- содержащих трехкомпонентных смесях. *Изв. вузов. Химия и хим. технология*. 2025. Т. 68. Вып. 6. С. 41–51. DOI: 10.6060/ivkkt.20256806.7181.

For citation:

Efremov A.M., Betelin V.B., Kwon K.-H. Influence of Ar/He ratio on plasma composition and silicon etching kinetics in CF_4- and C_4F_8- based ternary mixtures. *ChemChemTech* [*Izv. Vyssh. Uchebn. Zaved. Khim. Khim. Tekhnol*.]. 2025. V. 68. N 6. P. 41–51. DOI: 10.6060/ivkkt.20256806.7181.

INFLUENCE OF Ar/He RATIO ON PLASMA COMPOSITION AND SILICON ETCHING KINETICS IN CF_4- AND C_4F_8- BASED TERNARY MIXTURES

A.M. Efremov, V.B. Betelin, K.-H. Kwon

Alexander M. Efremov (ORCID 0000-0002-9125-0763)*

Molecular Electronics Research Institute (MERI), Academic Valiev st., 6/1, Zelenograd, Moscow, 124460, Russia
E-mail: amefremov@mail.ru

Vladimir B. Betelin (ORCID 0000-0001-6646-2660)

SRISA RAS, Nakhimovsky ave., 36, bld. 1, Moscow, 117218, Russia
E-mail: betelin@niisi.msk.ru

Kwang-Ho Kwon (ORCID 0000-0003-2580-8842)

Korea University, 208 Seochang-Dong, Chochiwon, Korea, 339-800
E-mail: kwonkh@korea.ac.kr

The investigation of plasma electro-physical parameters, gas phase composition and reactive-ion etching kinetics of silicon in CF_4 + Ar/He and C_4F_8 + Ar/He mixtures with variable ratio of inert components was carried out. The combination of plasma diagnostics tools (Langmuir probes, optical emission spectroscopy) with modeling of plasma chemistry allowed one a) to figure out how the Ar/He ratio influences densities of active species (fluorine atoms, polymerizing radicals and positive ions) determining the overall plasma-surface interaction result; b) to divide contributions of physical and chemical etching pathways; and c) to analyze the etching mechanism in terms of effective reaction probability. It was shown that the substitution of argon by helium produces several common features, such as a decrease in both electron temperature and electron density, a transition toward lower dissociation degrees for multi-atomic species that results in decreasing densities of less saturated fluorocarbon radicals and fluorine atoms as well as a fall of Si etching rate that follows the kinetics of heterogeneous reaction $Si + xF \rightarrow SiF_x$. The growth of corresponding reaction probabilities demonstrate an agreement with decreasing amount of deposited polymer in the case of CF_4 + Ar/He plasma, but contradicts with increasing polymerizing impact in C_4F_8 + Ar/He plasma. The last phenomenon probably reflects an enforcement of F atom flux (compared with that determined by F atom density in plasma) at the polymer/Si interface. The reason is the formation of F atoms in polymer layer of increasing thickness due to its de-fluorination by the ion bombardment.

Keywords: fluorocarbon gases, argon, helium, plasma, parameters, active species, ionization, dissociation, etching, reaction probability

INTRODUCTION

Gaseous or vaporized liquid fluorocarbon compounds have found numerous applications in plasma chemical processes used for cleaning and/or patterning (dimensional etching within a standard photolithography cycle) of many materials involved in the microelectronic technology. Among those, one can mandatory mention the silicon itself, silicon dioxide, silicon nitride and some metals featured by volatile fluorides [1-3]. The most comprehensive tool for such purposes is the reactive-ion etching (RIE) that combines physical (ions-induced sputtering) and chemical (spontaneous of ion-assisted chemical reaction) etching pathways. The relatively independent adjustment of corresponding process rates in inductively coupled plasma (ICP) reactors provides the effective optimization of output RIE characteristics (etching rate, etching selectivity in respect to mask material, degree of anisotropy and radial uniformity) according to given process requirements [3, 4]. That is why many technological processes using various fluorocarbon gas plasmas under the condition of low-pressure inductive rf (13.56 MHz) discharges have been developed.

When summarizing existing data on plasma chemistry of fluorocarbons [4, 5-8], one can conclude that a) the typical feature of any fluorocarbon gas is the deposition of polymer-like film at surfaces contacted with plasma; b) the polymerizing ability of given gas (in fact, both deposition rate and steady-state thickness of polymer film) depends on the carbon-to-fluorine

atom, C/F, ratio in original fluorocarbon molecule; and c) one of evident ways to adjust the polymerizing ability for given process requirements is to use binary gas mixtures with argon. In particular, the addition of argon lowers the polymer deposition rate through decreasing densities of polymerizing CF_x ($x < 3$) radicals as well as increases the gasification of deposited film due to an increase in ion bombardment intensity. That is why there were many experimental and theoretical (model-based) works dealt with binary gas mixtures combining fluorocarbon component with argon. Results of these works related to widely used fluorocarbon compounds, such as CF_4, CHF_3 and C_4F_8 [8-15], allowed one to figure out internal mechanism determining the influence of fluorocarbon/argon mixing ratio on steady-state densities of plasma active species as well as to understand relationships between mixture composition and RIE kinetics through etching/polymerization balance. On this background, the almost negligible attention was attracted to binary mixtures of fluorocarbons with helium. At the same time, the interest to helium is caused by, at least, two reasons. First, helium is featured by the extremely high heat conductivity (~ 0.152 W/mK compared with ~ 0.0164 W/mK for Ar at 300 K [16]) that provides the effective heat transfer from bulk plasma to chamber walls. Probably, this flattens radial gas temperature profiles and thus, provides favorable conditions for obtaining more uniform etching for big-size wafers. And secondly, three are several experimental evidences that the use of He instead of Ar as a third component in $CF_4 + C_4F_8$ as mixture provides the decent etching anisotropy for SiO_2 in a combination with the amorphous carbon layer mask [17, 18]. Obviously, understanding the nature of this effect is the mandatory condition for the optimization of existing RIE technologies.

The general idea of this work was to compare electro-physical parameters, plasma composition and silicon etching kinetics in CF_4 + Ar/He and C_4F_8 + + Ar/He gas mixtures with variable inert gas ratios. The main attention was focused on a) plasma diagnostics to obtain electrons- and ions-related characteristics; b) plasma modeling to determine densities and fluxes of plasma active species; and c) to analyze RIE kinetics of silicon in the approximation of effective reaction probability. The choice of fluorocarbon gases was mainly caused by their sufficient differences in respects to both polymerizing ability [5-7] and F atom kinetics [7, 8]. The choice of silicon as the etched material was due to its well-studied etching mechanism in the fluorine-containing environments. In our opinion, such situation provides the better understanding of side factors influencing the etching kinetics.

EXPERIMENTAL AND MODELING DETAILS

Experimental setup and plasma diagnostics methods

Both plasma diagnostics and etching experiments were performed in the planar (equipped by the top-side flat coil) inductively coupled plasma (ICP) reactor known from our previous works [8, 13-15]. Plasma was excited using the 13.56 MHz rf power supply while another similar rf generator was matched with the chuck electrode to adjust the negative dc bias voltage ($-U_{dc}$) and thus, to control the ion bombardment energy (ε_i). Constant processing parameters were total gas pressure (p = 6 mtor), input power (W_{inp} = 700 W, or ~ 0.07 W/cm^3) and bias power (W_{dc} = 200 W). Initial compositions of CF_4 + Ar/He and C_4F_8 + Ar/He gas mixture was set by adjusting partial flow rate for individual within the constant total flow rate q = 40 sccm. Particularly, the fixed flow rate of 20 sccm for CF_4 or C_4F_8 provided their constant fractions of 50% while the second half in each case was composed by different fraction of Ar (y_{Ar}) and He (y_{He}). Accordingly, and increase in q_{He} from 0-18 sccm corresponded y_{He} = 0-45% He with the proportional decrease in y_{Ar} down to 5%. The remaining amount of Ar was necessary to provide the actinometry experiments.

Plasma diagnostics by double Langmuir probe (DLP2000, Plasmart Inc.) delivered information on electrons- and ions-related plasma parameters. The probe head was installed through the viewport on the chamber wall, was located at ~ 5 cm above the chuck electrode as well as was centered in its radial position. The treatment of current-voltage (I-V) curves according to Langmuir probe theory for low-pressure high-density plasmas [4, 19] yielded electron temperature (T_e) and ion current density (J_+). In order to reduce inaccuracies due to the polymerization on probe tips, we periodically performed the probe conditioning procedure in 50% Ar + 50% O_2 plasma for ~ 5 min. As a result, we obtained the decent similarity in plasma parameters obtained in a series of consequent measurements under one and the same plasma excitation conditions.

Plasma diagnostics by optical emission spectroscopy (AvaSpec-3648, JinYoung Tech) provided the information on F atom densities. For this purpose, we applied the standard actinometry procedure with F 703.8 nm (ε_{th} = 14.75 eV) and Ar 750.4 nm (ε_{th} = = 13.48 eV) emission maxima. The final equation was as

$$[F] = y_{Ar} N C_a (I_F/I_{Ar}), \quad (1)$$

where I_F and I_{Ar} are measured emission intensities for F and Ar atoms, respectively, $N = p/k_B T_{gas}$ is the total gas

density at the gas temperature of T_{gas} while C_a is the actinometrical coefficient that depends on corresponding wavelengths (λ), excitation rate coefficients (k_{ex}) and optical transition probabilities (A) [20, 21]. Parameters $k_{ex,F}$ and $k_{ex,Ar}$ were obtained through the integration of known excitation cross-sections [21] with Maxwellian electron energy distribution function (EEDF). Similarly to Ref. [21], we also obtained $C_a \approx$ const at T_e = 3-6 eV. The parameter T_{gas} was assumed to be independent on both type of fluorocarbon gas (as it was done in our previous work related to $CF_4 + C_4F_8 + Ar$ plasma [7] where the fairly good agreement between model and experiment was obtained) and Ar/He mixing ratio. The last assumption was based on the work of Hofmann et al. [22] that reported the comparison between gas temperatures in atmospheric pressure Ar and He plasmas. Though He plasma was found to be a bit "hotter", authors mentioned this result as somewhat overestimated due to features of experimental technique. That is why, when determining N value we used T_{gas} = 600 K, as was evaluated from direct measurements in Ar and CF_4 plasmas in similar ICP reactor at corresponding to our case gas pressure and input power density [23, 24].

Etching experiments were performed with fragments of standard Si (111) wafer. Etched samples with an average size of ~ 2×2 cm were located in the center chuck electrode, and the latter was thermally stabilized at ~ 20 °C. The small sample size allowed one to exclude the loading effect as well as to minimize the disturbance of gas-phase plasma parameters by etching products. In fact, we obtained no differences in plasma diagnostics data obtained without and with sample loading, and even with simultaneous loading of several samples. After the processing, etched depths, Δh, were measured using the surface profiler (Alpha-Step 500, Tencor). For this purpose, samples were partially masked by the photoresist (AZ1512, positive) with a thickness of ~ 1.5 μm. In preliminary experiments, it was found that the dependence of Δh on processing time, τ, demonstrates the nearly linear shape up to 5 min. Accordingly, for any τ < 5 min the steady-state etching regime surely take place while Si etching rate may simply be calculated as $R = \Delta h/\tau$.

Plasma modeling

To obtain the information on densities and fluxes of plasma active species, we applied a simplified 0-dimensional (global) model described in our previous works [8, 13-15]. The input parameters were experimental data on T_e and J_+ obtained at different Ar/He mixing ratios. The kinetic scheme (the set of reactions with corresponding rate coefficients) was taken from previous studies dealt with the modeling of CF_4 + Ar and C_4F_8 + Ar [9, 12] plasmas. As several authors have mentioned the adequate agreement between model-predicted and measured plasma parameters, the discussion about the content of kinetic scheme seems to be not an actual task, at least for the purpose of given study. In Tab. 1, we represented the reduced version of kinetic scheme aimed at supporting the discussion in Section 3. Accordingly, it includes only reactions with the principal influence of particle balance and/or needed to trace important reaction mechanisms.

Table1

Reduced reaction scheme in CF_4 + Ar/He and C_4F_8 + Ar/He plasmas

***Таблица 1.* Сокращенная схема процессов в плазме CF_4 + Ar/He и C_4F_8 + Ar/He**

Process		k	Process		k
1.	$C_4F_8 + e \rightarrow 2C_2F_4 + e$	$f(T_e)$	12.	$Ar + e \rightarrow Ar^+ + 2e$	$f(T_e)$
2.	$C_4F_8 + e \rightarrow C_3F_6 + CF_2 + e$	$f(T_e)$	13.	$He + e \rightarrow He^+ + 2e$	$f(T_e)$
3.	$C_3F_6 + e \rightarrow C_2F_4 + CF_2 + e$	$f(T_e)$	14.	$F_2 + CF_x \rightarrow CF_{x+1} + F$	$f(T_{gas})$
4.	$C_2F_4 + e \rightarrow 2CF_2 + e$	$f(T_e)$	15.	$CF_x + F \rightarrow CF_{x+1}$	$f(T_{gas})$
5.	$C_2F_x + e \rightarrow C_2F_x^+ + 2e$	$f(T_e)$	16.	$C_2F_4 + F \rightarrow CF_2 + CF_3$	$f(T_{gas})$
6.	$CF_x + e \rightarrow CF_{x-1} + F + e$	$f(T_e)$	17.	$CF_x \rightarrow CF_x(s)$	$f(\gamma)$
7.	$CF_x + e \rightarrow CF_{x-1}^+ + F + 2e$	$f(T_e)$		$CF_x(s) + F \rightarrow CF_{x+1}$	
8.	$CF_x + e \rightarrow CF_x^+ + 2e$	$f(T_e)$	18.	$F \rightarrow F(s)$	$f(\gamma)$
9.	$F_2 + e \rightarrow 2F + e$	$f(T_e)$		$F(s) + CF_x \rightarrow CF_{x+1}$	
10.	$F_2 + e \rightarrow F_2^+ + e$	$f(T_e)$		$F(s) + C_2F_x \rightarrow CF_{x+1}$	
11.	$F + e \rightarrow F^+ + 2e$	$f(T_e)$		$F(s) + F \rightarrow F_2$	

Similarly to our previous works [7, 8], modeling algorithm accounted for known features of low-pressure high-density inductive discharges. In particular, it was assumed that

– The electron energy distribution function is sufficiently contributed by equilibrium electron-electron collisions due to high ionization degree of gas species ($n_+/N > 10^{-4}$, where n_+ is the total density of

positive ions). Such situation allows one to use Maxwellian EEDF for electron-impact kinetics as well as to determine corresponding rate coefficients as functions of electron temperature: $k = AT_e^B \exp(-C/T_e)$. The parameters A, B and C for all electron-impact reactions included in the kinetic scheme are known from Refs. [9, 12].

– The low electronegativity of CF_4 and C_4F_8 plasmas half-diluted by inert has allows one to assume $n_+ \approx n_e$ and $n_-/n_e << 1$, where n_- and n_e are densities of negative ions and electrons [7-9, 12]. The reasons are, again, the high ionization degree of gas species as well as the low efficiency of dissociative attachment processes, as sources of negative ions, at low pressures. Such situation reveals

$$J_+ \approx 0.61 e n_+ (eT_e/m_i)^{1/2} \quad (2)$$

where $0.61n_+$ is the density of positive ions at the interface between bulk plasma and double electric layer surrounding the probe while m_i is the effective (ion-type-averaged) ion mass [7].

– The loss of F atoms and CF_x radicals on chamber walls follows the first-order recombination kinetics. Corresponding recombination probabilities, γ, were assumed to be independent on Ar/He ratio due to the nearly constant temperature of internal chamber wall. The last fact was indirectly confirmed by the monitoring of external wall temperature.

RESULTS AND DISCUSSION

Previously, we have compared plasma parameters and gas-phase compositions in CF_4 + Ar and C_4F_8 + Ar gas mixtures under identical processing conditions [7, 8, 10]. Results of these works demonstrated that the addition of Ar always a) disturbs electrons- and ions-related plasma parameters through the influence on both EEDF and formation/decay balance for charged species; b) increases the ion bombardment intensity, according to the change in $\varepsilon_i^{1/2}\Gamma_+$, where ε_i is the ion bombardment energy, and Γ_+ is the ion flux; and c) non-proportionally reduces the F atom density. The non-linear dependencies $[F] = f(y_{Ar})$ are due to increasing F atom formation frequencies in R6 and R7 (mostly in CF_4 + Ar plasma) and changes in their loss kinetics through R16 (mostly in C_4F_8 + Ar plasma).

From Tables 1 and 2, it can be seen that the substitution of Ar by He results in the similar influence on electrons- and ions-related parameters in CF_4 + Ar/He and C_4F_8 + Ar/He plasmas. Corresponding effects are a) a weak decrease in ion current density that means same behaviors of electron and positive ion densities; and b) a reduction of electron temperature that provides same changes in rate coefficients for inelastic electron-impact processes with $\varepsilon_{th} \geq 3/2T_e$, where ε_{th} is the threshold energy. The common reason is the sufficient difference in ionization rate coefficients for Ar ($k_{12} \sim 2.5 \cdot 10^{-10}$ cm^3/s at T_e = 3 eV) and He ($k_{13} \sim 2.7 \cdot 10^{-12}$ cm^3/s at T_e = 3 eV) atoms caused by corresponding dissimilarities in corresponding cross-sections (~ $1.3 \cdot 10^{-15}$ cm^2 for R12 vs. ~ $4.5 \cdot 10^{-16}$ см^2 for R13 at electron energy of 10 eV) and threshold energies (~ 15.8 eV for R12 vs. ~ 24.6 eV for R13) [25]. That is why the appearance of much harder-ionizing species reduces overall formation rates for positive ion and electrons. The related phenomenon is that the addition of He lowers dissociation degrees for multi-atomic species and thus, leads to growth of their fractions in a gas phase (Fig. 1). Accordingly, as prevailing electron energy loss channels are provided by collisions with various fluorocarbon components, an increase in the effective particle size escalates the energy loss and results in decreasing T_e.

Table 2

Electrons- and ions-related plasma parameters
***Таблица 2*. Параметры электронной и ионной компонент плазмы**

y_{He}, %	T_e, eV	J_+, mA/cm^2	$n_+ \approx n_e$, cm^{-3}	$-U_{dc}$, V	$\varepsilon_i^{1/2}\Gamma_+$
CF_4 + Ar/He					
0	3.2	1.30	$5.1 \cdot 10^{10}$	315	$1.23 \cdot 10^{18}$
25	2.9	1.21	$4.9 \cdot 10^{10}$	349	$1.21 \cdot 10^{18}$
45	2.5	1.04	$4.7 \cdot 10^{10}$	394	$1.09 \cdot 10^{18}$
C_4F_8 + Ar/He					
0	3.7	1.42	$5.6 \cdot 10^{10}$	291	$1.12 \cdot 10^{18}$
25	3.3	1.31	$5.4 \cdot 10^{10}$	337	$1.10 \cdot 10^{18}$
45	2.9	1.12	$5.2 \cdot 10^{10}$	383	$1.00 \cdot 10^{18}$

Fig. 1 represents model-predicted data on partial fractions of various positive ions inside n_+ value. The common feature is that dominant ionic species at $y_{He} = 0$ are always CF_x^+ and Ar^+ while the condition of $k_{12} >> k_{13}$ prevents the proportional substitution of Ar^+ by He^+. In particular, the addition of helium to CF_4 + + Ar/He plasma lowers the density of originally prevailing Ar^+ (as is pre-determined by $k_{12} > k_7$ under the equivalent CF_4 and Ar mixing condition), but causes an increase in $[CF_3^+]$ which finally takes the leading position at ~ 35% He (Fig. 1(a)). The last effect is provided by increasing rate of R7 (x = 4) due to increasing CF_4 density (Fig. 2(a)). Though the CF_3^+ ion is characterized by higher mass compared with argon, the situation is compensated by the appearance of much lighter He^+. As such, the effective ion molar mass, $M_i = m_i N_A$, demonstrates even the weak fall toward He-rich plasmas (44-38 for 0-45% He). In the case of C_4F_8 + Ar/He

mixture, densities of originally prevailing CF_2^+ and Ar^+ also exhibit opposite tendencies with increasing y_{He}, so that the domination of CF_2^+ takes place at any Ar/He ratio (Fig. 1(b)). When comparing Figs. 1(b) and 2(b), it can be understood that the growth of $[C_2F_3^+]$ and $[CF_2^+]$ as well as the condition of $[CF^+] \approx$ const contradict with changes in densities of corresponding neutral species. The reason is the multi-channel ionization process for C_2F_4 molecules, where the dominant reaction pathway in a form of R5 ($k_5 \sim 2.0 \cdot 10^{-10}$ cm^3/s for x = 4 at T_e = 3 eV) is accompanied by several parallel reactions schemes, such as $C_2F_4 + e \rightarrow C_2F_3^+ + F + 2e$ ($\sim 3.8 \cdot 10^{-11}$ cm^3/s at T_e = 3 eV), $C_2F_4 + e \rightarrow CF_2^+ + CF_2 + 2e$ ($\sim 3.6 \cdot 10^{-11}$ cm^3/s) and $C_2F_4 + e \rightarrow CF^+ + CF_3 + + 2e$ ($\sim 2.2 \cdot 10^{-11}$ cm^3/s). Such situation provides the nearly constant effective ion molar mass, about 45-48 at 0-45% He. Therefore, the intensity of ion bombardment vs. y_{He} in both gas mixtures is definitely not affected by M_i, but is determined by opposite behaviors of ion bombardment energy ε_i (as follows from the change in $-U_{dc}$, see Tab. 1) and ion flux $\Gamma_+ \approx J_+/e$ within the parameter $\varepsilon_i^{1/2}\Gamma_+$. As the latter demonstrates the weak decrease (in CF_4 + Ar/He plasma) or keeps a nearly constant value (in C_4F_8 + Ar/He plasma), one can surely assume no principal influence of Ar/He ratio on kinetics of ion-induced heterogeneous processes.

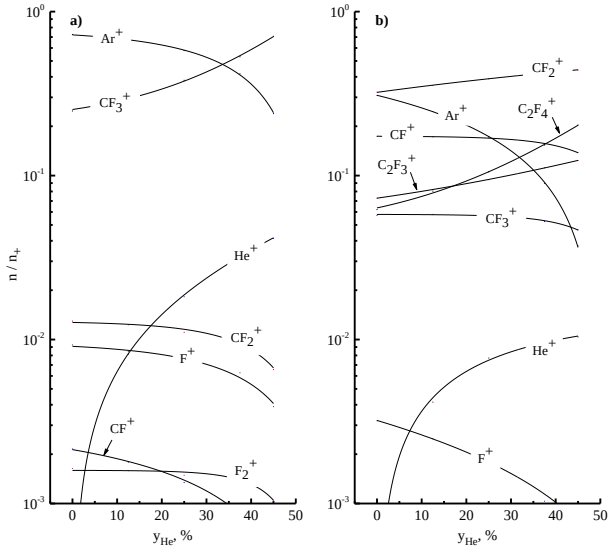

Fig. 1. Model-predicted fractions of positive ions inside n_+ in CF_4 + Ar/He (a) and C_4F_8 + Ar/He (b) plasmas

Рис. 1. Расчетные доли положительных ионов в составе n_+ в плазме CF_4 + Ar/He (a) и C_4F_8 + Ar/He (b)

When analyzing kinetics of neutral species, we surely confirmed earlier reported features of non-oxygenated CF_4- and C_4F_8-based plasmas [8-10, 12, 14, 26]. In first case, dominant fluorine-containing species in a gas phase are original CF_4 molecules, CF_3 radicals and F atoms (Fig. 2(a)). Accordingly, the main F atom formation channels compiling ~ 80% of total F atom formation rate are represented by R6 (x = 3, 4) and R7 (x = 4). As both processes with a participation of CF4 also produce CF_3 radicals, the condition of $[F] \approx [CF_3]$ reasonably takes place. In addition, the mostly stepwise (from higher- to lower-saturated species) formation of CF_x trough R6 results in $[CF_x] > [CF_{x-1}]$. The last fact has been reported by many authors dealt with experimental and theoretical (model-based) studies of CF_4-based plasmas (see, for example, Refs. [9, 12]). The loss of both CF_x (x < 4) and F species appears through heterogeneous processes R17 and R18. As the latter produces F_2 molecules featured by high dissociation rate coefficient ($\sim 1.8 \cdot 10^{-9}$ cm^3/s for k_9 compared with $\sim 1.0 \cdot 10^{-10}$ sm^3/s for k_6 with x = 4 at T_e = 3 eV), the contribution of R9 to the total F atom formation rate reaches ~ 10%. The feature of C_4F_8-based plasma is the complete decomposition of original C_4F_8 molecules through the sequence of R1–R5 into CF_x (x = 1, 2) and C_2F_x (x = 3, 4) products (Fig. 2(b)). Accordingly, the main source of F atoms is R6 for x = 1-3 while their loss in R16 has the comparable rate with that for a sum of R16 and R17. That is why 50% C_4F_8 + 50% Ar plasma exhibits higher F atom formation rate together with a bit lower F atoms density compared with the corresponding CF_4-based mixture.

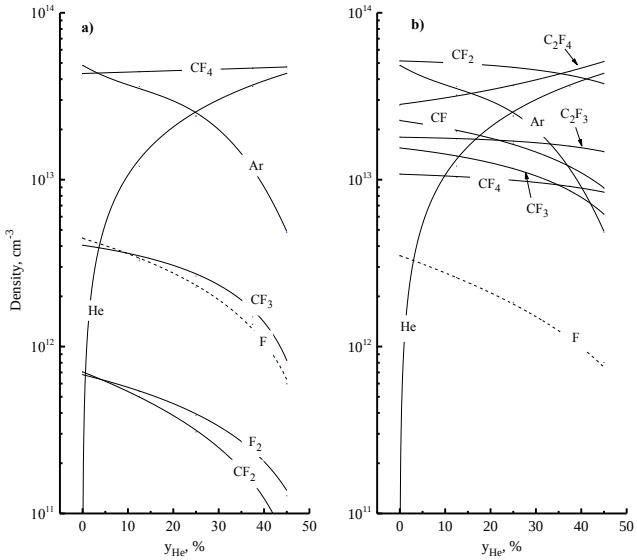

Fig. 2. Model-predicted densities of neutral species in CF_4 + Ar/He (a) and C_4F_8 + Ar/He (b) plasmas

Рис. 2. Расчетные концентрации нейтральных частиц в плазме CF_4 + Ar/He (a) и C_4F_8 + Ar/He (b)

The substitution of Ar by He does not modify and/or bring new processes in above reaction schemes, but retards the electron-impact dissociation of multiatomic species due to the simultaneous decrease in T_e

and n_e. Accordingly, both gas mixtures exhibit increasing densities of original molecules (or their first-step decomposition product, in the case of C_4F_8) and decreasing density of F atoms toward He-rich plasmas. As for F atom kinetics, a decrease in $(k_6+k_7)n_e$ for CF_4 molecules in CF_4 + Ar/He appears as 13.6-2.1 s^{-1}, or by ~ 6.5 times for 0-45% He while the corresponding change in k_6n_e for CF_2 in C_4F_8 + Ar/He is only by ~ 2 times, from 68.8-31.9 s^{-1}. Therefore, the deeper fall in corresponding dissociation frequencies in the case of CF_4 + Ar/He plasma produces the stronger response from the side of [F] value, as can be seen from Fig. 2. Another remarkable fact is that model-predicted densities of F atom are in the satisfactory agreement with those obtained by actinometry experiments in both CF_4 + Ar/He and C_4F_8 + Ar/He plasmas (Fig. 3(a, b)). Taking into account that F atoms kinetics is closely matched with all kinds of fluorocarbon species, one can assume correct model-based description of plasma chemistry in given gas systems. The latter means that model-predicted data on plasma composition may surely be used for etching kinetics analysis.

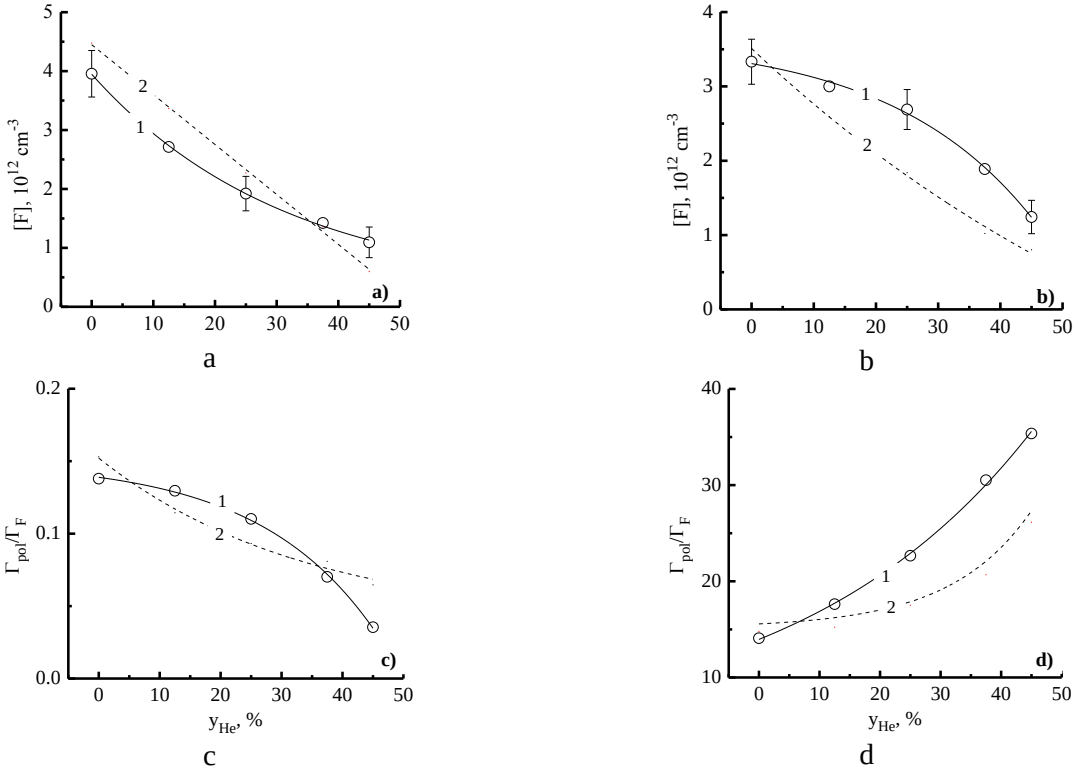

Fig. 3. Gas-phase plasma characteristics influencing Si etching kinetics in CF_4 + Ar/He (a, c) and C_4F_8 + Ar/He (b, d) plasmas. In Figs. a, b): F atoms densities determined form actinometry experiments (1) and plasma modeling. In Figs. c, d): the parameter Γ_{pol}/Γ_F tracing plasma polymerization ability determined using measured (1) and model-predicted (2) densities of F atoms

Рис. 3. Характеристики газовой фазы, влияющие на кинетику травления кремния в плазме CF_4 + Ar/He (a, c) и C_4F_8 + Ar/He (b, d). На рис. a, b): концентрации атомов фтора, определенные методом актинометрии (1) и при моделировании плазмы (2). На рис. c, d): параметр Γ_{pol}/Γ_F, отслеживающий полимеризационную способность плазмы, определенный с использованием экспериментальной (1) и расчетной (2) концентрации атомов фтора

From Refs. [4-7], it can be understood that output RIE characteristics (etching rate, etching selectivity in respect to mask material and etching anisotropy) in fluorocarbon-based plasmas sufficiently depend on both plasma polymerizing ability and etching/polymerization balance. Numerous studies of polymerization kinetics allowed one to conclude that a) main polymerizing species are CF_x (x = 1, 2) radicals; and b) the polymerization is retarded in fluorine-rich plasmas. The latter is because F atoms saturate free bonds on the film surface and thus, break the growth of polymer chains [5, 6]. That is why the polymer deposition rate and polymer film thickness may adequately be traced by Γ_{pol}/Γ_F ratio, where Γ_{pol} is the total flux of polymerizing radicals, and Γ_F is the flux of F atoms [7, 8]. From Figs. 3(c, d), one can conclude that C_4F_8-bases plasma is originally much more polymerizing gas system (as it predicted by higher C/F ratio and has been confirmed in many experiments) while the substitution of Ar by He exhibits an opposite effect on the parameter Γ_{pol}/Γ_F. The latter means that a transition toward He-rich plasmas lowers the polymer deposition rate in CF_4 + Ar/He

plasma (due to the stronger fall of Γ_{pol} compared that for Γ_F) while causes an increase of polymerizing ability in C_4F_8 + Ar/He plasma (due to much weaker decreasing Γ_{pol} on the background of Γ_F). The last phenomenon is because of $[CF_2] \approx$ const, as produced by the nearly constant rate of R4 due to opposite changes in n_e and C_2F_4 density.

Etching experiments indicated that the substitution of Ar by He lowers Si etching rates, R, in the nearly linear manner (187-151 nm/min in CF_4 + Ar/He and 125-100 nm/min in C_4F_8 + Ar/He at 0–45% He, see Fig. 4(a, b)). The evaluation sputter etching component as $R_{phys} = Y_S\Gamma_+$, where Y_S is the sputter yield (0.18-0.39 atom/ion at ε_i = 200-400 eV [27]), gives ~ 31 nm/min for CF_4 + Ar/He plasma and ~ 33 nm/min for C_4F_8 + Ar/He plasma. Therefore, the condition of $R_{phys} << R$ evidently means the domination of chemical etching pathway. From Figs. 4(a, b), it can be seen also that the rate heterogeneous chemical reaction $R_{chem} = R - R_{phys}$ contradicts with the change in $\varepsilon_i^{1/2}\Gamma_+$ (and thus, with the ion bombardment intensity), but formally follows the decreasing tendency of F atom flux, Γ_F. Such situation reveals no ion-driven limiting stages in the multi-step chemical etching process as well as assumes the neutral-flux-limited etching regime. In fact, such situation looks quite expectable, as the silicon spontaneously reacts with F atoms with a formation of volatile SiF_4 [4]. The analysis of reaction kinetics with model-predicted fluxes of F atoms leads to following conclusions:

– In CF_4 + Ar/He plasma, a decrease in R_{chem} appears to be weaker compared with Γ_F, that points out on increasing effective reaction probability, $\gamma_R = R_{chem}/\Gamma_F$ (Fig. 4(c)). The given change of γ_R also contradicts with the ion bombardment intensity, but shows the reasonable agreement with decreasing polymer deposition rate, as shown in Fig. 3(c). Really, even if the low polymerizing CF_4 plasma does provide the formations of thick continuous polymer film on Si surface, the decreasing amount of deposited polymer increases the amount of free adsorption sites for F atoms and thus, accelerates the consequent reaction scheme $F \rightarrow F(s.)$; $xF(s.) + Si \rightarrow SiF_x(s.)$; $SiF_x(s.) \rightarrow SiF_x$ through its first stage.

– In C_4F_8 + Ar/He plasma, one can easily expect the formation of thick continuous film that limits the access of F atoms to the etched surface. On this background, an increase in γ_R (Fig. 4(d)) together with increasing both polymer deposition rate (Fig. 3(d)) and film thickness (that evidently causes the worse access of etchant species to the target material) looks a bit surprisingly. As the given phenomenon cannot be explained within above heterogeneous reaction mechanism, one can assume the presence of side factors influencing the chemical etching kinetics. In our opinion, the quite realistic reason may be the so-called "defluorination effect" which accounts for the formation of additional (in respect to those coming from a gas phase) F atoms in bulk polymer under the ion bombardment [5, 6]. In particular, Ref. [5] reported that the silicon with preliminary deposited thick polymer film exhibits typically chemical etching rates under the Ar^+ ion bombardment. Therefore, one can assume that increasing polymer film thickness in a combination with the condition of $\varepsilon_i^{1/2}\Gamma_+ \approx$ const enlarges the ion path inside the polymer layer, causes an increase in the amount of newly generated F atoms and provides the relative growth of F atom flux on the polymer/silicon surface interface.

In order to confirm above suggestions concerning etching mechanism, we conducted a series of experiments with variable bias power. It was found that the change in W_{dc} has no principal (i.e. exceeding the standard experimental error) influence on both Langmuir probe diagnostics result and plasma emission spectra. The latter surely means no disturbance of gas-phase plasma characteristics as well as allows one to assume Γ_+, Γ_{pol} and $\Gamma_F \approx$ const, at least within the investigated range of W_{dc} = 200-500 W. In fact, this finding reflects the typical feature for ICP etching systems to provide the independent control for ion flux and ion bombardment energy [4]. Accordingly, the single evident effect from the growth of bias power in both gas systems is the nearly linear increase in negative dc bias voltage, ion energy and ion bombardment intensity (Table 3). As a result, one can reasonably account for increasing polymer decomposition rate by ion bombardment and thus, for decreasing polymer film thickness. The latter follows from the change in $\Gamma_{pol}/\varepsilon_i^{1/2}\Gamma_+\Gamma_F$ ratio (Table 3) that was previously suggested to trace the amount of residual polymer in oxygen-free fluorocarbon plasmas [7, 8, 10].

Etching experiments indicated that an increase in W_{dc} accelerates the Si etching process, lowers the gap between R_{phys} and R_{chem}, but finally did not break the rule of $R_{chem} > R_{phys}$ even at maximum W_{dc} value. In particular, the transition toward higher bias powers in CF_4 + Ar/He plasma changes the Si etching rate from 187-281 nm/min under He-free conditions as well as in the range of 151-190 nm/min at y_{He} = 45% (Fig. 5(a)). As both effects are mainly provided by corresponding changes in R_{chem}, the condition of $\Gamma_F \approx$ const directly means an increase in effective reaction probabilities,

γ_R. In our opinion, the most realistic reason is exactly same as has been suggested to explain the effect of Ar/He ratio. Really, one can easily imagine that an increase in ion bombardment intensity lowers the amount of residual polymer and accelerates the chemical etching pathways through increasing amount of vacant adsorption sites for F atoms. That is why the change in both γ_R and R_{chem} appears to be weaker in He-rich plasmas, as it is featured by lower polymerizing ability.

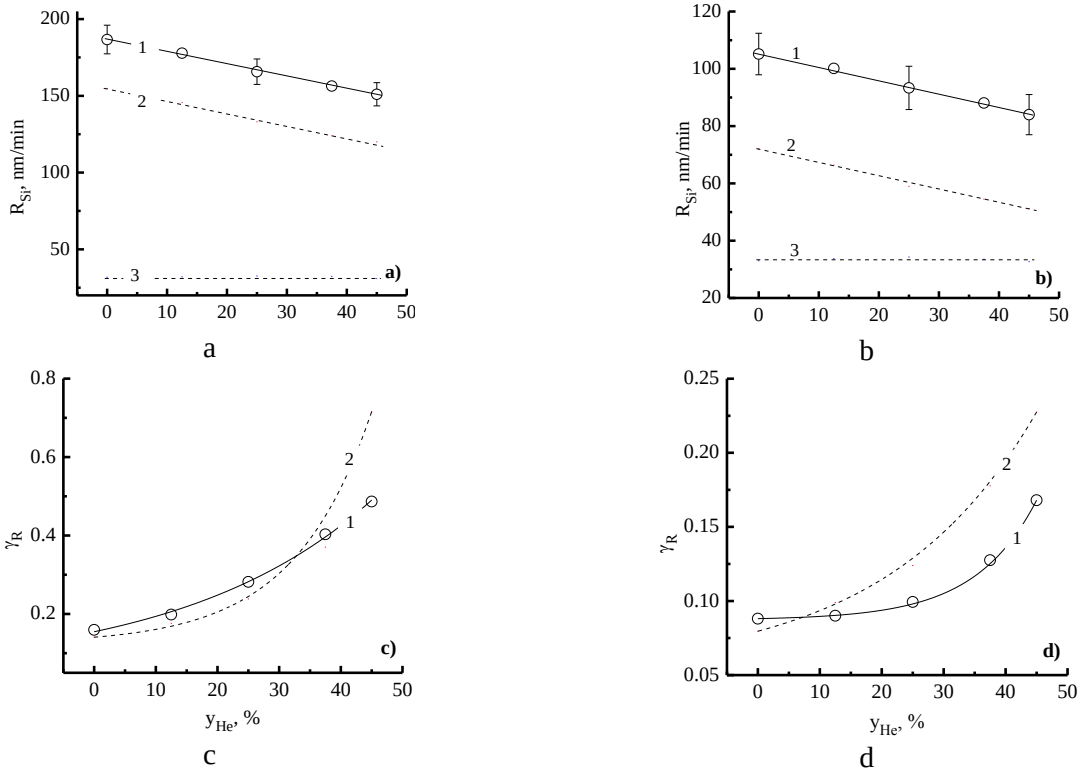

Fig. 4. Silicon etching rate (a, b) and effective probability of heterogeneous Si + xF → SiF_x reaction (c, d) in CF_4 + Ar/He (a, c) and C_4F_8 + Ar/He (b, d) plasmas. In Figs. a, b): 1 – measured etching rate; 2 – rate of heterogeneous chemical reaction; and 3 – rate of physical sputtering. In Figs. c, d): 1 – γ_R determined using measured F atom density; 2 – γ_R determined using model-predicted F atoms density

Рис. 4. Скорость травления кремния (a, b) и эффективная вероятность гетерогенной реакции Si + xF → SiF_x (c, d) в плазме CF_4 + Ar/He (a, c) и C_4F_8 + Ar/He (b, d). На рис. a, b): 1 – измеренная скорость травления; 2 – скорость гетерогенной химической реакции; и 3 – скорость физического распыления. На рис. c, d): 1 – γ_R, определенная по экспериментальной концентрации атомов фтора; 2 – γ_R, определенная по расчетной концентрации атомов фтора

Table 3

Effect of bias power on gas-phase parameters tracing ion-driven process kinetics

***Таблица 3*. Влияние мощности смещения на параметры газовой фазы, отслеживающие кинетику ионно-стимулированных процессов**

y_{He}, %	0	45	0	45	0	45
W_{dc}, W	-U_{dc}, V		$\varepsilon_i^{1/2}\Gamma_+$, 10^{18}		$\Gamma_{pol}/\varepsilon_i^{1/2}\Gamma_+\Gamma_F$, 10^{-19}	
CF_4 + Ar/He						
200	315	394	1.23	1.09	0.95	0.55
500	498	569	1.53	1.31	0.70	0.42
C_4F_8 + Ar/He						
200	291	383	1.30	1.14	108	210
500	460	530	1.65	1.39	87	175

In C_4F_8 + Ar/He plasma, an increase in W_{dc} leads to much weaker growth of Si etching rate (105-119 nm/min at 0% He and 84-95 nm/min at 45% He and 200-500W, see Fig. 5(b)) that is mainly provided by increasing R_{phys}. Accordingly, the condition of R_{chem} ≈ const directly means $\gamma_R \approx$ const. The last phenomenon probably suggests that the positive effect from decreasing polymer thickness (as follows from increasing ion bombardment intensity at $\Gamma_{pol}/\Gamma_F \approx$ const) is compensated by the negative one that inhibits the heterogeneous chemical reaction. The non-contradictive explanation assumes the weakening of de-fluorination effect due to decreasing ion path inside the polymer film. This lowers the chemically active "add-on" from the side of "secondary" F atoms and thus, reduces the efficiency of chemical reactions on the polymer/Si surface interface. Therefore, similarly to CF_4 + Ar/He plasma, effects of Ar/He ratio and bias power also allow the universal explanation.

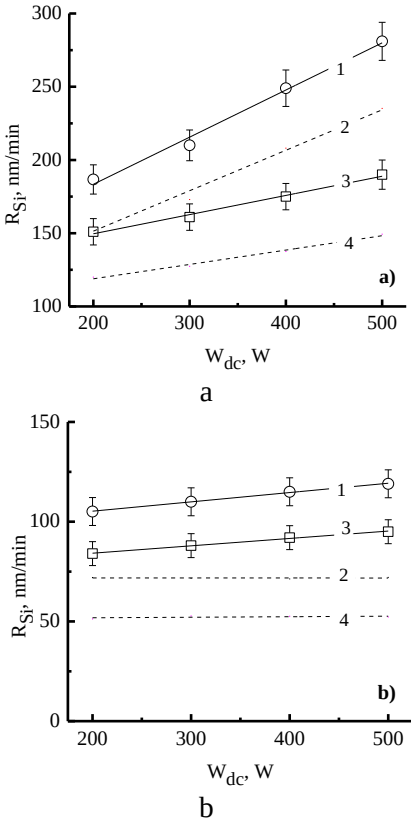

Fig. 5. Silicon etching rate as a function of bias power in CF_4 + Ar/He (a) and C_4F_8 + Ar/He (b) plasmas at y_{He} = 0% (1, 2) and y_{He} = 45% (3, 4). Dashed lines correspond to R_{chem}

Рис. 5. Скорость травления кремния в зависимости от мощности смещения в плазме CF_4 + Ar/He (a) и C_4F_8 + Ar/He (b) при y_{He} = 0% (1, 2) и y_{He} = 45% (3, 4). Пунктирные линии соответствуют R_{chem}

Definitely, we understand that above explanations for C_4F_8 + Ar/He plasma look rather speculative, as these are not directly confirmed by experiments. At the same time, corresponding suggestions do not contradict with general regularities of plasma chemistry, account for really existing physical effect and were based on verified plasma modeling data. As for the last argument, the positive sign is also that parameters Γ_{pol}/Γ_F and γ_R exhibit similar behavior being determined using model-predicted or measured F atom densities. The latter means no uncertainty in the interpretation of etching data as well as increases the confidence that related conclusions are principally correct.

This study is a part of the FNEF-2024-0004 government order contracted to the Scientific Research Institute for System Analysis of the National Research Centre «Kurchatov Institute», project No. 1023032900380-3-1.2.1 "Fundamental and applied research in the field of lithographic limits of semiconductor technologies and physicochemical processes of etching 3D nanometer dielectric structures for the development of critical technologies for the production of electronic components. Research and construction of models and designs of microelectronic elements in an extended temperature range (from -60 ℃ to +300 ℃) (FNEF-2024-0004)".

The authors declare the absence of a conflict of interest warranting disclosure in this article.

Работа выполнена в рамках государственного задания НИЦ «Курчатовский институт» - НИИСИ по теме № FNEF-2024-0004, проект No. 1023032900380-3-1.2.1 «Фундаментальные и прикладные исследования в области литографических пределов полупроводниковых технологий и физико-химических процессов травления 3D нанометровых диэлектрических структур для развития критических технологий производства ЭКБ. Исследование и построение моделей и конструкций элементов микроэлектроники в расширенном диапазоне температур (от -60 ℃ до +300 ℃)».

Авторы заявляют об отсутствии конфликта интересов, требующего раскрытия в данной статье.

REFERENCES
ЛИТЕРАТУРА

1. **Wolf S., Tauber R.N.** Silicon Processing for the VLSI Era. Volume 1. Process Technology. New York: Lattice Press. 2000. 416 p.
2. **Nojiri K.** Dry etching technology for semiconductors. Tokyo: Springer Internat. Publ. 2015. 116 p. DOI: 10.1007/978-3-319-10295-5.
3. Advanced plasma processing technology. New York: John Wiley & Sons Inc. 2008. 479 p.
4. **Lieberman M.A., Lichtenberg A.J.** Principles of plasma discharges and materials processing. New York: John Wiley & Sons Inc. 2005. 757 p. DOI: 10.1002/0471724254.
5. **Standaert T.E.F.M., Hedlund C., Joseph E.A., Oehrlein G.S., Dalton T.J.** Role of fluorocarbon film formation in the etching of silicon, silicon dioxide, silicon nitride, and amorphous hydrogenated silicon carbide. *J. Vac. Sci. Technol. A.* 2004. V. 22. P. 53-60. DOI: 10.1116/1.1626642.
6. **Stoffels W.W., Stoffels E., Tachibana K.** Polymerization of fluorocarbons in reactive ion etching plasmas. *J. Vac. Sci. Tech. A.* 1998. V. 16. P. 87-95. DOI: 10.1116/1.581016.
7. **Efremov A., Son H.J., Choi G., Kwon K.-H.** On Mechanisms Influencing Etching/Polymerization Balance in Multi-Component Fluorocarbon Gas Mixtures. *Vacuum.* 2022. V. 206. P. 111518. DOI: 10.1016/j.vacuum.2022.111518.
8. **Efremov A., Lee B. J., Kwon K.-H.** On relationships between gas-phase chemistry and reactive-ion etching kinetics for silicon-based thin films (SiC, SiO_2 and Si_xN_y) in multi-component fluorocarbon gas mixtures. *Materials.* 2021. V. 14. P. 1432. DOI: 10.3390/ma14061432.
9. **Kimura T., Ohe K.** Probe measurements and global model of inductively coupled Ar/CF_4 discharges. *Plasma Sources Sci. Technol.* 1999. V. 8. P. 553-561. DOI: 10.1088/0963-0252/8/4/305.
10. **Efremov A.M., Murin D.B., Kwon K.-H.** Concerning the Effect of Type of Fluorocarbon Gas on the Output Characteristics of the

Reactive-Ion Etching Process. *Russ. Microelectronics*. 2020. V. 49. N 3. P. 157-165. DOI: 10.1134/S1063739720020031.
11. **Proshina O., Rakhimova T.V., Zotovich A., Lopaev D.V., Zyryanov S.M., Rakhimov A.T.** Multifold study of volume plasma chemistry in Ar/CF_4 and Ar/CHF_3 CCP discharges. *Plasma Sources Sci. Technol.* 2017. V. 26. P. 075005. DOI: 10.1088/1361-6595/aa72c9.
12. **Rauf S., Ventzek P.L.** Model for an inductively coupled Ar/c-C_4F_8 plasma discharge. *J. Vac. Sci. Technol. A.* 2002. V. 20. P. 14-23. DOI: 10.1116/1.1417538.
13. **Efremov A.M., Murin D.B., Kwon K.-H.** Features of the Kinetics of Bulk and Heterogeneous Processes in CHF_3 + Ar and C_4F_8 + Ar Plasma Mixtures. *Russ. Microelectronics*. 2019. V. 48. N 2. P. 119-127. DOI: 10.1134/S1063739719020070.
14. **Ефремов А.М., Мурин Д.Б., Квон К.Х.** Параметры плазмы и кинетика активных частиц в смеси CF_4+C_4F_8+Ar. *Изв. вузов. Химия и хим. технология.* 2018. Т. 61. Вып. 4-5. С. 31−36. **Efremov A.M., Murin D.B., Kwon K.H.** Plasma parameters and active species kinetics in CF_4+C_4F_8+Ar gas mixture. *ChemChemTech [Izv. Vyssh. Uchebn. Zaved. Khim. Khim. Tekhnol]*. 2018. V. 61. N 4-5. P. 31-36. DOI: 10.6060/tcct.20186104-05.5695.
15. **Ефремов А.М., Бетелин В.Б., Медников К.А., Kwon K.-H.** Параметры газовой фазы и режимы реактивно-ионного травления Si и SiO_2 в бинарных смесях Ar + CF_4/C_4F_8. *Изв. вузов. Химия и хим. технология.* 2021. Т. 64. Вып. 6. С. 25-34. **Efremov A.M., Betelin V.B., Mednikov K.A., Kwon K.-H.** Gas-phase parameters and reactive-ion etching regimes for Si and SiO_2 in binary Ar + CF_4/C_4F_8 mixtures. *ChemChemTech [Izv. Vyssh. Uchebn. Zaved. Khim. Khim. Tekhnol.]*. 2021. V. 64. N 6. P. 25-34. DOI: 10.6060/ivkkt.20216406.6377.
16. Handbook of Chemistry and Physics. New York: CRC Press. 2014. 2704 p.
17. **Choi G., Efremov A., Lee D.-K., Cho C.-H., Kwon K.-H.** On Mechanisms to Control SiO_2 Etching Kinetics In Low-Power Reactive-Ion Etching Process Using CF_4 + C_4F_8 + Ar + He Plasma. *Vacuum*. 2023. V. 216. P. 112484. DOI: 10.1016/j.vacuum.2023.112484.
18. **Choi G., Efremov A., Son H. J., Kwon K.-H.** Noble gas effect on ACL etching selectivity to SiO_2 films. *Plasma Process. Polym.* 2023. V. 20. N 8. P. e2300026. DOI: 10.1002/ppap.202300026.
19. **Shun'ko E.V.** Langmuir probe in theory and practice. Boca Raton: Universal Publishers. 2008. 245 p.
20. **Engeln R., Klarenaar B., Guaitella O.** Foundations of optical diagnostics in low-temperature plasmas. *Plasma Sources Sci. Technol.* 2020. V. 29. P. 063001. DOI: 10.1088/1361-6595/ab6880.
21. **Lopaev D.V., Volynets A.V., Zyryanov S.M., Zotovich A.I., Rakhimov A.T.** Actinometry of O, N and F atoms. *J. Phys. D: Appl. Phys.* 2017. V. 50. P. 075202. DOI: 10.1088/1361-6463/50/7/075202.
22. **Hofmann S., van Gessel A.F.H., Verreycken T., Bruggeman P.** Power dissipation, gas temperatures and electron densities of cold atmospheric pressure helium and argon RF plasma jets. *Plasma Sources Sci. Technol.* 2011. V. 20. P. 065010. DOI: 10.1088/0963-0252/20/6/065010.
23. **Cunge G., Ramos R., Vempaire D., Touzeau M., Neijbauer M., Sadeghi N.** Gas temperature measurement in CF_4, SF_6, O_2, Cl_2, and HBr inductively coupled plasmas. *J. Vac. Sci. Technol. A.* 2009. V. 27(3). P. 471-478. DOI: 10.1116/1.3106626.
24. **Celik Y., Aramaki M., Luggenholscher D., Czarnetzk U.** Determination of electron densities by diode-laser absorption spectroscopy in a pulsed ICP. *Plasma Sources Sci. Technol.* 2011. V. 20. P. 015022. DOI: 10.1088/0963-0252/20/1/015022.
25. **Raju G.G.** Gaseous electronics. Tables, Atoms and Molecules. Boca Raton: CRC Press. 2012. 790 p. DOI: 10.1201/b11492.
26. **Ефремов А.М., Бобылев А.В., Kwon K.-H.** Параметры плазмы и кинетика травления кремния в смеси CF_4+ C_4F_8+ O_2: эффект соотношения CF_4/C_4F_8. *Изв. вузов. Химия и хим. технология.* 2024. Т. 67. Вып. 6. С. 29-37. **Efremov A.M., Bobylev A.V., Kwon K.-H.,** Plasma parameters and silicon etching kinetics in CF_4 + C_4F_8 + O_2 mixture: effect of CF_4/C_4F_8 mixing ratio. *ChemChemTech [Izv. Vyssh. Uchebn. Zaved. Khim. Khim. Tekhnol.]*. 2024. V. 67. N 6. P. 29-37. DOI: 10.6060/ivkkt.20246706.6982.
27. A Simple Sputter Yield Calculator. https://www2.iap.tuwien.ac.at/www/surface/sputteryield (30.11.2024).

Поступила в редакцию 06.12.2024
Принята к опубликованию 04.02.2025

Received 06.12.2024
Accepted 04.02.2025